TECHNICAL UNIVERSITY OF CLUJ-NAPOCA

ACTA TECHNICA NAPOCENSIS

Series: Applied Mathematics, Mechanics, and Engineering
Vol. 67, Issue Special IV, August, 2024

FRICTION AT THE GRAIN-SCALE: THE ROLE OF INTER-PARTICLE FRICTION IN GRANULAR MEDIA AND ITS EFFECT ON GRAIN-AND-MACRO-SCALE BED BEHAVIOUR

Jack MOSS, Romeo GLOVNEA

Abstract: *In these experimental lab-based tests, 'dry' and 'wet' ideal granular beds, consisting of quasi-2D polydisperse discs, are harmonically compressed via a moving sidewall and their responses captured via high-speed imaging. First, the behaviour of a 'dry' granular bed is examined, and then a thin layer of glycerol is spread onto the edges of each individual disc for the behaviour of a 'wet' granular bed to be examined. The individual behaviour of these beds is analysed and compared. In general, the reduced friction in the wet granular bed leads to more sliding and less rolling at the grain-scale, which in turn produces greater ease of macro-scale bed deformation. These results are used to discuss the role of inter-particle friction in granular behaviour.*

Key words: *Granular matter, experimental, quasi-2D, multiphase physics, soft matter*

1. INTRODUCTION

Granular media, such as soils, rocks, sands, grains, powders and more, is ubiquitous in nature and is the second most processed substance in industry after water. It has become the focus of a steadily growing area of literature in recent decades on account of its ability to exhibit a wide variety of phenomena under different loading conditions, for example, compaction [1][2][3] or convection at the grain-scale under vibrational load [4][5][6]. When part or all of a granular bed is sufficiently agitated, the net result is spatial displacement of constituent particles and energy transfer within the granular material [7][8][9].

Existing literature firmly establishes that the behaviour of a granular system at the continuum-scale is fundamentally governed by grain-scale interactions between neighbouring particles [10][11][12]. Away from the free surface of an agitated granular bed, the dominant grain-scale interactions are relative sliding and rolling between neighbouring particles [13], and it is this sliding and rolling which is the subject of this paper.

One dry and one lubricated, or 'wet', ideal granular bed is subjected to cyclic rapid compressions by a harmonically oscillating sidewall, and the resulting granular behaviour is captured via high-speed imaging. The ideal beds consist of discs of five different diameters, or 'species', and each disc has a straight line crossing its diameter to enable disc rotation to be tracked. Several Matlab scripts were written to locate and track each disc through each test. The behaviour of the dry and wet granular beds are compared, and the results used to discuss the extent to which friction governs inter-particle interactions at the grain-scale.

2. EXPERIMENTAL PROCEDURE

The tests performed for this paper are pleasingly simple in principle. Evenly mixed test beds of discs, one dry and one lubricated with glycerol, are subjected to cyclic rapid compression from the moving left-wall of the tank they were contained within. This process is filmed with a high-speed camera; the captured images forming the core of the raw experimental data.

2.1 Experimental Apparatus

A labelled photograph of the core components of the experimental apparatus can be seen in Fig. 1. The apparatus was bolted to an optical table,

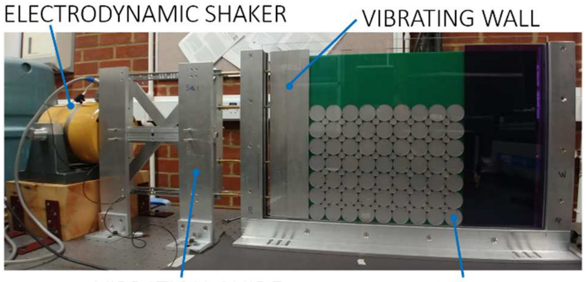

Fig. 1. Core experimental apparatus

with the exception of the camera, which was mounted on a tripod on the ground.

The ideal quasi-2D granular media consisted of discs of five diameters, 36.2*mm*, 27.1*mm*, 21.2*mm*, 15.0*mm*, and 12.0*mm*, cut from 3.1*mm* polyurethane sheets. Each disc had a line drawn across its face to enable its rotation to be tracked.

Due to the discs having little mass, vibrofluidisation (where particles in a vibrated bed have relative free movement in air and interact primarily via instantaneous collisions) was a concern. To address this, a 'floating roof' was constructed, as shown in Fig. 2. The term 'floating' refers to the fact the roof is not fixed in place but merely resting on the bed of discs.

This roof was laser-cut from 3*mm* acrylic in the profile of a randomly distributed bed of discs and then evenly weighted with 220*g*. The floating nature and organic shape allows the packing structure of the discs at the top of the bed to reach a natural arrangement and avoids constraining the media to a fixed area. The observed behaviour of the disc-bed in these tests

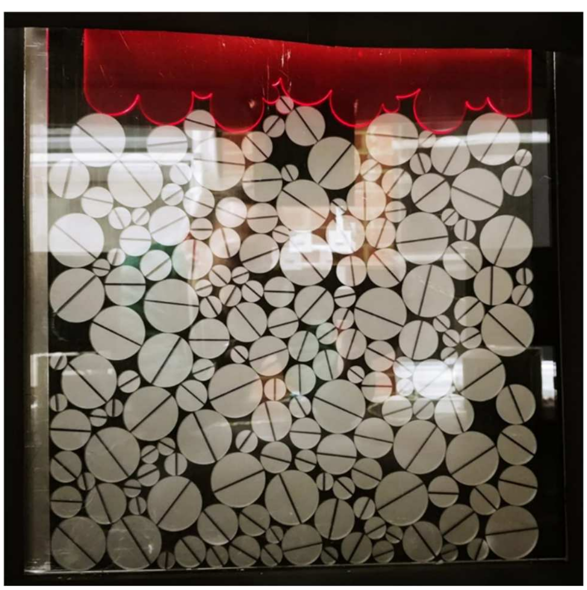

Fig. 2. Typical test bed with the floating roof

can thus be viewed as the behaviour of the bottom layers of a much deeper bed, where vibrofluidisation is at a minimum.

The body of the tank was made from aluminium, with the bed for the discs being 326*mm* x 400*mm* x 3.5*mm*.

To drive the vibrations, an LDS V406 electrodynamic shaker was connected to the left sidewall via a linear-bearing guide rail to avoid any vertical component to the vibrations.

To help avoid parallax distortion in the images, the Phantom MIRO C211 camera was placed 2.5*m* away from the tank and an adjustable zoom lens was used.

High speed imaging is sensitive to lighting conditions because any lighting inconsistencies will be captured by the high framerate of the camera, even if they are not noticeable to the human eye. For these tests, four arrays of high-power LEDs were custom built, combining to provide upwards of 12,000 Lumens of consistent DC light at full power. This brightness level enabled the camera shutter speed to be reduced to 182μs to eliminate motion blur in the images. Natural light was blocked from the laboratory to maintain consistent lighting regardless of weather, and the region between the camera and viewing window was cloaked in black fabric to eliminate external reflections.

A load cell was installed between the shaker and the moving left-wall of the tank and monitored by a GW-Instek GDS-2064 digital oscilloscope. A simple DC switch was wired into the oscilloscope and used to power a high-low trigger in the camera. When triggered, the camera records, and the oscilloscope captures 12,500 data points from the load cell. In this way, each individual image from the tests can be synchronised with the load-cell data, and the exact point in the vibration cycle for that image can be determined.

2.2 Procedure

To load the tank, one disc of each species was randomly dropped until the bed was approximately 350*mm* deep. This produced a randomly packed, but evenly mixed, ideal granular bed containing just over 30 of each of the five species of disc – about 160 discs in total. To prevent anomalous bed deformation arising from instability in the initial packing structure, the beds were gently agitated for 30*s* to allow rearrangement to a more stable internal structure. The floating roof was then placed in position.

For the wet tests, the only difference in set up procedure was that each individual disc had a thin coating of undiluted glycerol spread onto the surface of its perimeter before being dropped into the tank. Care was taken to avoid glycerol touching either face of a disc.

To begin each experiment, the vibrating wall was activated and the bed was left for 5*s* to allow it to reach a 'steady state' before the camera and oscilloscope began recording.

For both the dry and wet beds, a 32*s* test was performed to capture flow characteristics over a long period, before a 2*s* test at 1792*fps* was performed for high temporal resolution. Test conditions are stated in table 1.

Table 1

Test conditions for the granular beds.

	Peak-to-peak amplitude (*mm*)	**Frequency (*Hz*)**	**Frame rate (*fps*)**	**Duration (*s*)**
Dry	6	16	112	32
Dry	6	16	1792	2
Wet	6	16	112	32
Wet	6	16	1792	2

3. IMAGE PROCESSING AND DISC IDENTIFICATION

Each of the four tests produced 3584 images. To automate data extraction, Matlab scripts were written. The sequential steps for data extraction are listed below.

1. Original test images are captured and saved
2. Lighting adjustments and area of interest cropping
3. Circle finding algorithm for disc identification
4. 'Cleanup' algorithm including disc tracking
5. Quantitative data extraction

In the following, the design of these scripts is outlined, including the various Matlab functions used. Technical details regarding these functions are omitted but references to the MathWorks Matlab Help Centre is given lest more detail is required.

3.1 Initial Image Adjustments

The first script simply cropped to the viewing window, brightened, increased the contrast, and converted from 12*bit* colour to 16*bit* greyscale. This optimised the images for the next script: the circle finding algorithm.

3.2 The Circle Finding Algorithm

The circle finding algorithm is the most important script for data extraction, since all subsequent data handling relies on the discs being located correctly. The method chosen for circle detection was the Hough Transform because of a combination of its relative robustness, reliability, and its usability in Matlab with the *imfindcircles()* [14] function.

imfindcircles() takes a radius range in pixels and a sensitivity from 0-1 and 'searches' for sharp changes in pixel intensity in the shape of an arc with the specified radius range. The sensitivity value required to find a circle in an image is arbitrary and depends on various factors unique to each image, including the radius of the circle, the completeness of the circle, the contrast between the background and the circle, and the bit depth of the image. As such, no single sensitivity can be expected to find all circles within an image without error: an algorithm is required. The algorithm written for this research requires the following:

- The image
- A list of the number of discs of each species within the image
- A list of radius ranges for each disc species

While decidedly non-trivial to implement, the principle behind the circle finding algorithm, henceforth called *circle_finder*, is simple.

For each image, *circle_finder* starts with a baseline sensitivity for the Hough Transform and searches for discs of each species in turn. For each successfully located disc, it saves the disc radius, coordinates of the disc centre, and exports the pixels to file. To avoid duplicate disc detection, detected discs are 'deleted' from the image by blacking out their pixels.

When no more discs can be found, the algorithm checks the number of discs found against the input list of the number discs in the image. If there are more to be found, the process is repeated with the sensitivity increased by a small increment.

This cycle is repeated until all discs within the image have been found. The output files - lists containing the disc pixels and location information for each image - are saved.

3.3 'Cleanup' algorithm and disc tracking

As can be expected from locating 160 discs in over 3,500 separate images, erroneous disc identification is inevitable and a 'cleanup' algorithm required. The errors from *circle_finder* fall into two categories: additional 'false' circles are identified, or some actual discs are missed. The circle finding algorithm was designed to avoid incidence of the latter. Across four tests and 14,336 images, over 2 million individual circles needed locating and a combined total of only 29 circles were missed. This gives the circle finding algorithm written for this research a success rate vanishingly close to 100%.

However, this reliability comes at the price of sometimes finding additional false circles. It was empirically found that these false circles are found when the sensitivity of the Hough Transform was highest, thus, the first step in the cleanup algorithm, *disc_cleanup*, is simply to eliminate all circles listed after the 160th circle located in each image.

The next step in *disc_cleanup* is to identify all discs at the top of the frame and remove them from the list if they are only partially within shot. Only discs which are fully captured within the frame are useful for analysis because partial discs cannot have their location and angle reliably determined.

The final step of *disc_cleanup* is to track the discs between frames by assigning 'disc numbers'. The assumption at the root of the disc tracking algorithm is that discs do not move many pixels between images. The algorithm for tracking discs is thus pleasingly simple: a disc in image number n must be the same as the nearest disc of the same species in image $(n - 1)$. Any discs not located by *circle_finder* in a test image are flagged by the disc tracking algorithm and subsequently deleted from the list of discs to be analysed in that test.

The output files from *disc_cleanup* are lists of discs in each image which are wholly within shot and tracked through all frames in the test. These are used for data extraction.

4. DATA EXTRACTION

Since the frame rate is known, the time between each frame, $\triangle t$, is also known. High frame rates, small timesteps, and known locations for the discs in each frame yield powerful data extraction capability. The data extracted for each disc in each test is listed below, and the calculation methods are described in this section.

- Angle
- Angular distance
- Angular velocity
- Angular acceleration
- Resultant torque
- Linear distance
- Linear velocity
- Linear acceleration
- Resultant force

4.1 Angle calculation

The image of each disc (saved during the running of *circle_finder*) is loaded and binarised to maximise brightness and contrast. This optimises the clarity of the black line denoting the angle. A Gaussian filter is applied to reduce noise in the image.

The Matlab function *edge()* [15] is then used to find the sharp edges in the image. The output of *edge()* is a black-and-white image showing only the outlines of the objects in the original image: in this case, the outline of the disc and the line crossing its diameter.

The circular outline of the disc is cropped out of the image so only the lines spanning the diameter remain. At this stage, a Hough

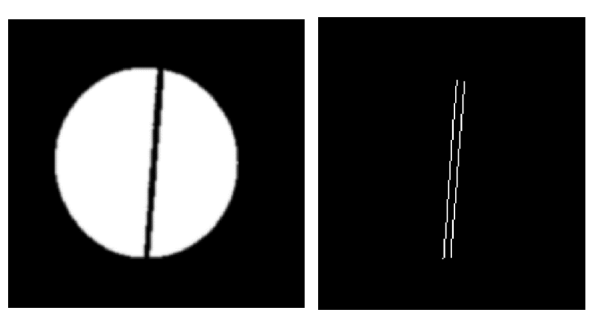

(a). Binarised pixels of a disc **(b).** Isolated disc lines

Fig. 3. Disc angle determination: lines extracted from binary image

transform is again applied, this time to identify the pixels showing the line drawn on each disc. Once located, the angle is determined. This image adjustment process is demonstrated in Fig. 3.

4.2 Time-dependent variables

All time-dependent variables were calculated using a central differencing temporal discretisation scheme.

Time and/or spatial discretisation methods are covered in depth in many Computational Fluid Mechanics books, such as [16]. In the interests of conciseness, a derivation of the formulas is omitted here. The first-and-second derivative formulas are given below in equations (1) and (2), using known values up to the current time. The case of linear distance, s, is used for convenience; these formulas hold true for any time-dependent variable and its derivatives. Velocity and acceleration at time t are denoted $v(t)$ and $a(t)$ respectively. Time $(t-1)$ is the time in the previous timestep, and so on.

$$v(t-1/2) = s'(t-1/2) \approx \frac{s(t)-s(t-1)}{\Delta t} \quad (1)$$

$$a(t-1) = s''(t-1) \approx \frac{s(t)-2s(t-1)+s(t-2)}{\Delta t^2} \quad (2)$$

These finite differencing methods were used for all four tests in this paper. Equivalent equations were used for the rotational movement of each disc. This produces velocity values a half-timestep behind each frame: this is no issue, since velocity changes over the whole duration of each test are examined.

Once angular and linear acceleration were determined, it was possible to determine resultant torque and resultant force on each disc, since the mass and moment of inertia of each disc species is known. These equations are performed for all ∼150 discs tracked through each of the 3584 frames in all four tests.

5. RESULTS AND DISCUSSIONS

Qualitatively, it is possible to see from the videos of each test that the lubricated beds are less agitated than the dry beds. There is no convective effect - that is to say, each disc remains broadly in the same location throughout the duration of each test. Most discs simply oscillate diagonally, with some rotation. Each load cycle, the lower-right region of the dry bed appears to exhibit ‘jamming’ - where closely packed particles ‘lock’ and exhibit larger-than-usual resistance to deformation - before deforming as the left-wall compresses the bed further. The wet bed does not do this, and although the discs are less agitated in the wet bed, a greater proportion of the bed appears to deform. The degree of agitation in differing regions of each bed, usually referred to as the granular temperature, is difficult to tell from qualitative analysis alone. Likewise, the degree to which the dry bed is more agitated than the wet bed is hard to see from viewing the videos.

With this in mind, granular temperature plots were generated to provide an intuitive visual insight into these variations. These plots are shown in Fig. 4. Before considering these plots, it should be noted that granular temperature is a

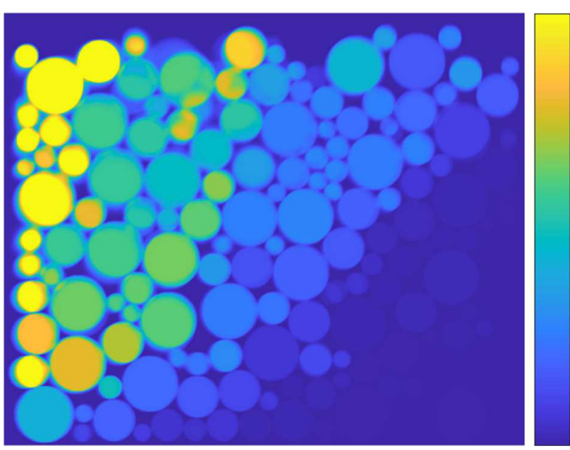

(a). Dry bed

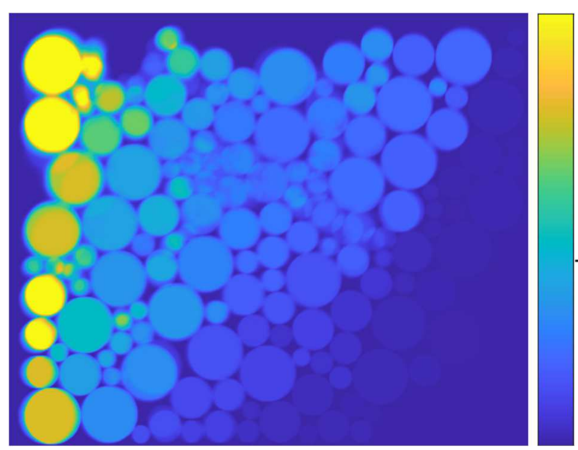

(b). Wet bed

Fig. 4. Granular temperature variation through the beds

concept derived from statistical mechanics and does not always have an easy interpretation like temperature in thermodynamics. To take a random example, direct numeric comparison of granular temperature values of a grain of sand and a block of granite will not yield straightforward, or even sensible, physical interpretations. In the case of Fig. 4, the images have equivalent colour scales which is sufficient for direct comparison to one another. The granular temperature distribution in the beds matches qualitative expectations based on existing literature [12].

Three characteristics are clear from Fig. 4, the most obvious being that the degree of agitation of a disc is dependent on the region of the bed it sits within, and independent of its species or size. Put simply, the closer to the moving wall a disc is, the greater its granular temperature.

Secondly, there are no sharp changes in granular temperature between neighbouring discs in either bed. The two triangular regions demonstrate well how the granular material on a macro scale exhibits a shearing motion at an angle from the direction of the applied load. In the dry case this angle is close to 45°, but it is closer to 60° in the lubricated case.

Thirdly, the dry bed is quantitatively more agitated than the wet bed.

The greater degree of agitation in the dry bed coupled with the difference in angle of the shearing motion leads to interesting deductions regarding the grain-scale interactions between neighbouring discs. The lubrication of the contact points will, of course, reduce the static friction at each contact, in turn reducing the jamming effect at the grain scale. Rather than jamming leading to sudden initial movement and high granular temperature, the discs in the lubricated bed appear to move more gently: at the macro-scale, linear movement penetrates deeper through the width of the bed away from the driving wall, increasing the shearing angle, but at the grain-scale, the discs themselves do not move with a high degree of agitation.

It is natural to now investigate a rotational equivalent of granular temperature distribution. Fig. 5. displays this.

It is immediately clear that well-defined regions of rapidly spinning discs within the bed do not exist and that rotational energy is more dependent on the disc's size than its geographic location. There are a few outliers, but in general, the smaller discs rotate more than the larger. This observation is in line with existing literature [17]. There is not much difference in disc rotation between the two tests close to the driving wall, but across the whole width, the dry bed again exhibits greater disc movement - although it's unclear from Fig. 5 exactly how much greater. In both there appears to be networks of rotating smaller discs weaving between the larger discs; a phenomenon which also aligns with the literature [18]. In the dry bed this network reaches further: there are small discs with a high degree of rotation far from the driving wall, in the upper right-hand region.

To investigate further the manner in which the dry bed is more agitated than the wet, the magnitude of the linear distance the discs travelled as they oscillated was summed, and then averaged across the bed. Fig. 6 shows this.

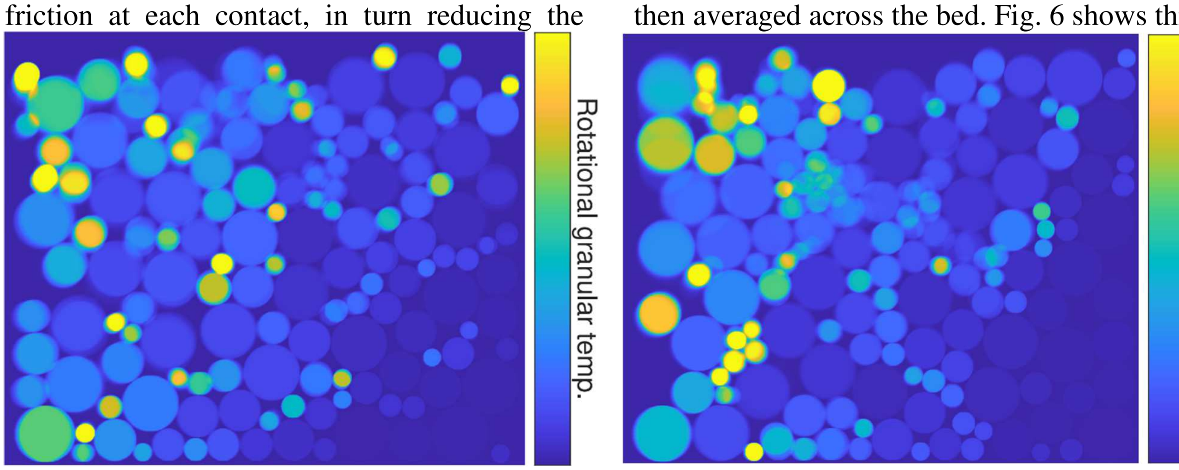

(a). Dry bed

(b). Wet bed

Fig. 5. Rotational equivalent of granular temperature variation through the beds

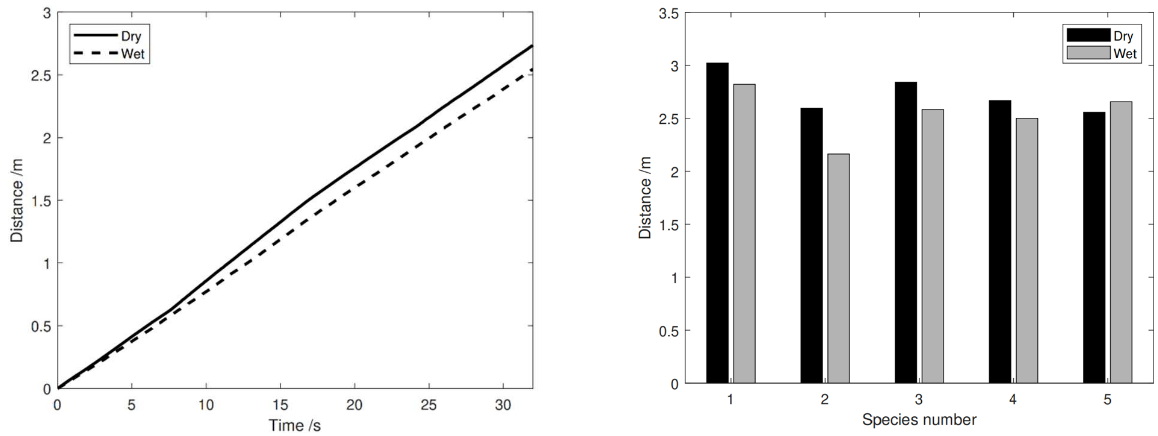

(a). Distance moved progression through each test

(b). Average distance moved per species

Fig. 6. Linear distance sums through each test. Species 1 is largest, 5 the smallest. Dotted lines in figure (a) denote the wet test, solid lines the dry test.

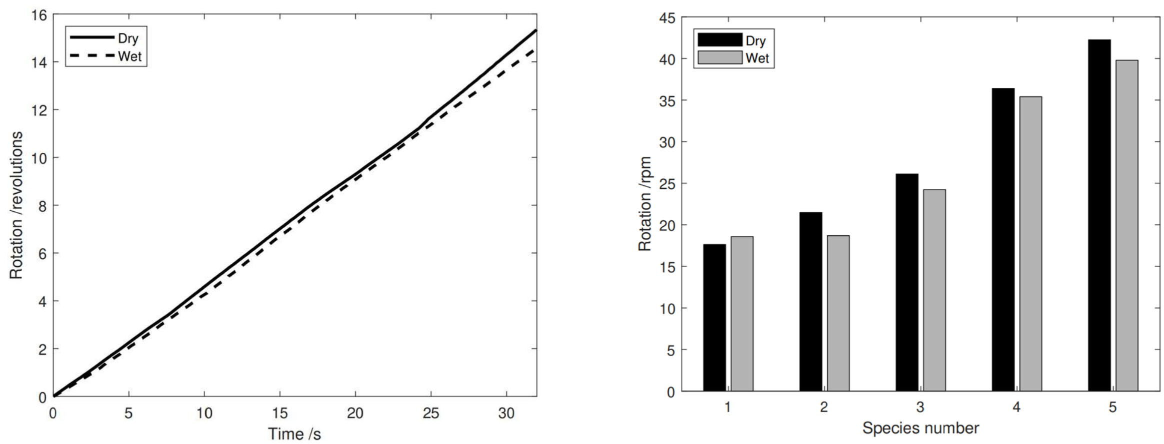

(a). Number of full revolutions progression

(b). Average rate of rotation per species

Fig. 7. Disc rotation through each test. Species 1 is largest, 5 the smallest. Dotted lines in figure (a) denote the wet test, solid lines the dry test.

Fig. 6(a) shows the dry bed exhibits greater linear movement than the lubricated bed, aligning with the deductions from Fig. 4. Total disc movement in each bed grows linearly from zero to a maximum value. Fig. 6(b) demonstrates that there is not a large variation, nor a distinct pattern, in distance moved when comparing between each species. Fig. 6(b) also shows how the largest four species move more in the dry bed.

The fact that species 5 (the smallest discs) move more in the lubricated bed is interesting. The difference is small; indeed it is the smallest difference in movement out of all the species. It is the view of the authors that this discrepancy can be attributed to a combination of their size and the nature of the granular temperature distribution in the bed. Being the smallest means they require the least force to be physically moved, and although the lubricated bed has a lower degree of agitation as a whole, movement within the bed propagates further from the driving wall, activating a larger number of discs despite the lower granular temperature at the macro-scale. While perhaps unintuitive, this would explain the contradictory behaviour of the smallest discs.

The rotational equivalent of Fig. 6 is shown in Fig. 7. Again aligning with earlier deductions, Fig. 7 indicates that disc size is the most important factor in rotational energy. In both the wet and the dry tests, the smaller the disc, the more it rotates. Similar to linear movement, the rotational movement of each disc increases linearly throughout the duration of the test. The discrepancy with species 1 rotating more in the

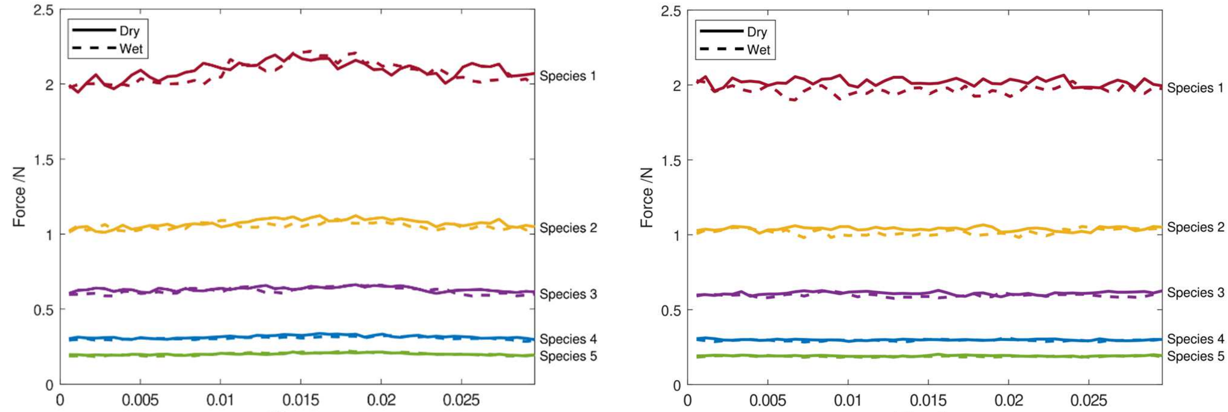

(a). Compression phase of load cycle **(b).** Relaxation phase of load cycle

Fig. 8. Resultant force average per load cycle on each disc species. Dotted lines denote the lubricated tests, solid lines the dry tests.

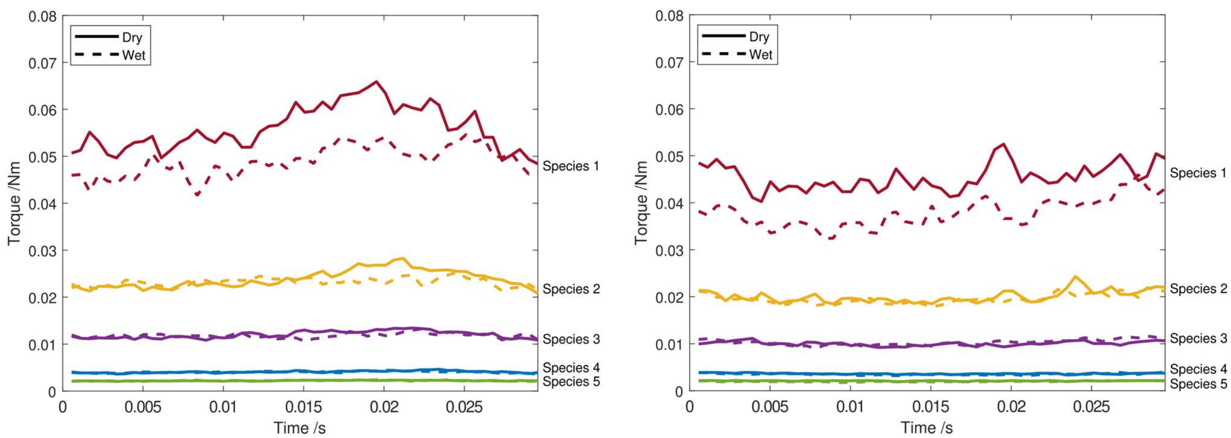

(a). Compression phase of load cycle **(b).** Relaxation phase of load cycle

Fig. 9. Resultant torque average per load cycle on each disc species. Dotted lines denote the lubricated tests, solid lines the dry tests.

lubricated tests is attributed to the random packing arrangement of the beds themselves. Fig. 5.(b) shows two discs of species 1 in the upper left corner; the most linearly and rotationally agitated region of the bed. These two discs weigh the average shown in Fig. 7. They have not been excluded, however, because the authors' view is that it is important for Fig. 5.(b) and 7 to directly correlate.

It is evident so far that the vibrating load from the wall stimulates diverse behavioural responses at the grain-scale from each disc, dependent on both its size and its geographic location. Seeking greater understanding of these behavioural responses, the load cycle the beds are subjected to are examined. The load cycle is split into two phases: compression and relaxation. The average resultant force on each species of disc through the duration of the compression and relaxation phase is presented in Fig. 8.

Before analysis of these graphs, some understanding of the typical shapes they may display is required. Numeric force values are, in effect, acceleration values scaled for mass, since $F = ma$. Thus, for equivalent movement, the largest discs will inherently have the largest resultant force, and the smallest disc species the smallest resultant force. In the specific case of these results, Fig. 8 displays the combined scalar magnitude of x and y force values - so a perfectly flat line would simply represent gravitational acceleration.

This, in essence, is what is shown to be happening during the relaxation phase of the load cycle in Fig. 8(b). By comparison, the force-curve for each species in the compression phase is bow shaped, denoting variable acceleration with time. This is true for all five disc species, although the effect is only slight for the smaller discs.

The shape matches expectations: the vibrating wall moves sinusoidally and is at its fastest in the middle of the compression, before decelerating towards maximum compression and subsequent relaxation.

It is interesting to note that the discs in the lubricated bed are subjected to resultant forces that are only marginally smaller, in general, than the discs in the dry bed. The differences in macro-scale bed behaviour become increasingly marked with time, leading to the observation that these small differences in each individual load cycle sum together with their effect on macro-scale bed properties only seen after many load cycles.

The rotational equivalent of Fig. 8, torque progression on each disc species averaged across each load cycle, is shown in Fig. 9. These plots require similar interpretation to their linear counterparts, in that a flat line denotes free-rolling with gravity and no slip.

The most striking feature of Fig. 9. is the difference in torque on the largest disc species through the entire load cycle, even in the relaxation phase. Viewed in context with the granular temperature results at the macro-scale, this points to increased sliding at the grain scale in the lubricated bed. There is a slight upwards bow-shape to the torque-curves of the largest three disc species during compression, and a slight downwards bow-shape during relaxation. This non-constant and alternating torque pattern loosely matches the sinusoidal load case, but 90 degrees out of phase.

When undergoing compression, the torque values and resultant force values increase, suggesting that, under compressive load, the discs linearly move past one another while also spinning. However, during the relaxation phase, Fig. 8.(b) points to the discs moving through space under constant gravitational acceleration. This makes the drop in resultant torque through relaxation phase particularly compelling because it points to a decrease in incidence of rolling during relaxation. It is known that relative movement at the grain-scale consists of a combination of both sliding and rolling [13]; the evidence from these results implies greater incidence of rolling during the compression phase of a load cycle, and greater incidence of sliding during the relaxation phase.

Regarding the smallest two species: since they occupy less physical space than the largest three species, they have the highest probability of having free space around them while the bed is agitated. They also have a smaller surface area with which to be contacted by neighbouring discs. It is likely, therefore, being in contact with fewer neighbouring discs leads to reduced opportunity for inconsistent torques to be imposed upon them; accounting for their flatter torque-curves.

The final note from both Figs. 8 and 9 is that both resultant force and torque are always greater than zero throughout the whole duration of each full load cycle. The net result of the fluctuating load imposed by the vibrating wall is a state of consistent agitation within the bed.

6. CONCLUSIONS

Grain-scale responses to external load vary. Both disc size and location within a bed can affect the behaviour of individual discs with rotation being more dependent on size and linear movement more dependent on location. The addition of lubrication reduces static friction at interparticle contacts, in turn reducing incidence of jamming often seen in granular matter. This lowers the level of agitation of each disc, corresponding with a lowering of the granular temperature. Somewhat unintuitively, there is more linear movement in discs far from the driving-wall and a greater proportion of the bed is deformed at the macro-scale in the wet bed.

Smaller torque and resultant force values through the whole load cycle correlate with the differing macro-scale behaviour of the lubricated and un-lubricated beds. In comparison with the dry bed, the lubricated bed moved more ‘sluggishly’, with smaller linear and angular movement of constituent discs. This gives fantastic insight into the effect of lubrication on grain-scale interactions: with reduced friction, neighbouring discs impose smaller torques onto one another and instead of rolling, slide past one another far more easily. Summed across the whole bed, this has a marked effect on macro-scale granular behaviour.

7. REFERENCES

[1] E. Clement and J. Rajchenbach. Fluidization of a bidimensional powder. Europhysics Letters, 16(2):133–138, 1991.

[2] L. Olmos, J.-M. Chaix, S. Nadler, O. Bonnefoy, J.-L. Gelet, and G. Thomas. Study by x-ray microtomography of the horizontal vibration effects on sand densification. Granular Matter, 18:61, 2016.

[3] A Raihane, O. Bonnefoy, J.-M. Chaix, J.-L. Gelet, and G. Thomas. Analysis of the densification of a vibrated sand packing. Powder Technology, 208:289–295, 2011.

[4] Kurt Liffman, G. Metcalfe, and P. Cleary. Granular convection and transport due to horizontal shaking. Physical Review Letters, 79(23):4574–4576, 1997.

[5] S-S. Hsiau, M-Y. Ou, and C-H Tai. The flow behaviour of granular material due to horizontal shaking. Advanced Powder Technology, 13(2):167–180, 2002.

[6] C. Zeilstra, J. G. Collignon, M. A. van der Hoef, N. G. Deen, and J. A. M. Kuipers. Experimental and numerical study of wall-induced granular convection. Powder Technology, 184(2):166–176, 2008.

[7] T. Hua and R. A. Van Gorder. Wave propagation and pattern formation in two-dimensional hexagonally-packed granular crystals under various configurations. Granular Matter, 21:3, 2019.

[8] L.-L. Li, X.-Q Yang, and W. Zhang. Two interactional solitary waves propagating in two-dimensional hexagonal packing granular system. Granular Matter, 20:49, 2018.

[9] A P. Awasthi, K. J.Smith, P. H. Geubelle, and J. Lambros. Propagation of solitary waves in 2d granular media: A numerical study. Mechanics of Materials, 54:100–112, 2012.

[10] S. Singh and T. G. Murthy. Evolution of structure of cohesive granular ensembles in compression. International Journal of Solids and Structures, 238(1):111359, 2022.

[11] M. Oda, J. Konishi, and S. Nemat-Nasser. Experimental micromechanical evaluation of strength of granular materials: effects of particle rolling. Mechanics of Materials, 1(4):269–283, 1982.

[12] Z. Benson, A. Peshkov, D. Richardson, and W. Losert. Effects of interparticle friction on the response of 3D cyclically compressed granular material. EPJ Web of Conferences, 249:10003, 2021.

[13] J. Moss and R. Glovnea. Behavioural responses to horizontal vibrations of quasi-2D ideal granular beds: an experimental approach. Granular Matter, 25:63, 2023.

[14] MathWorks. Matlab *imfindcircles*. https://uk.mathworks.com/help/images/ref/imfindcircles.html, 2024.

[15] MathWorks. Matlab *edge*. https://uk.mathworks.com/help/images/ref/edge.html, 2024.

[16] J. H. Ferziger and M. Peric. **Computational Methods for Fluid Dynamics**. Springer, NY, 2002.

[17] B. Dai, J. Yang, C Y. Zhou. Observed Effects of Interparticle Friction and Particle Size on Shear Behavior of Granular Materials. International Journal of Geomechanics, 16(1):04015011, 2015.

[18] M. Kuhn, and K. Bagi. Particle rotations in granular materials. ASCE EM Conference, 2002.

Reibung im granularen Maßstab: Die Rolle der Reibung zwischen Partikeln in granularen Medien und ihre Auswirkungen auf das Verhalten im granularen- und makroskopischen Maßstab im Bettenverhalten

In diesen experimentellen labortechnischen Tests werden ‚trockene' und ‚feuchte' ideale granulare Medien, bestehend aus quasi-2D polydispersen Scheiben, harmonisch durch eine sich bewegende Seitenwand komprimiert und ihre Reaktionen mittels Hochgeschwindigkeitsbildgebung erfasst. Zunächst wird das Verhalten eines ‚trockenen' granularen Mediums untersucht, sodann wird eine dünne Schicht Glycerin an den Rändern jeder einzelnen Scheibe aufgetragen, um das Verhalten eines ‚feuchten' granularen Mediums zu untersuchen. Das individuelle Verhalten dieser Medien wird analysiert und verglichen. Im Allgemeinen führt die reduzierte Reibung im feuchten granularen Medium zu mehr Gleiten und weniger Rollen auf der Ebene des Granulats, was wiederum eine stärkere makroskopischen Verformung des Materials erleichtert. Diese Ergebnisse werden verwendet, um die Rolle der Partikelreibungswechselwirkung im Verhalten von Granulaten zu diskutieren.

Jack Moss*, University of Sussex, j.t.moss@sussex.ac.uk. *Corresponding author
Romeo Glovnea, Professor, University of Sussex, r.p.glovnea@sussex.ac.uk.